

Strong, Fracture-Resistant Biomimetic Silicon Carbide Composites with Laminated Interwoven Nanoarchitectures Inspired by the Crustacean Exoskeleton

Mingyang Zhang,^{†,‡} Da Jiao,[†] Guoqi Tan,^{†,‡} Jian Zhang,^{†,§} Shaogang Wang,[†] Jingyang Wang,^{†,‡} Zengqian Liu,^{*,†,‡} Zhefeng Zhang,^{*,†,‡} and Robert O. Ritchie^{*,||} 

[†]Materials Fatigue and Fracture Division, Institute of Metal Research, Chinese Academy of Sciences, Shenyang 110016, China

[‡]School of Materials Science and Engineering, University of Science and Technology of China, Hefei 230026, China

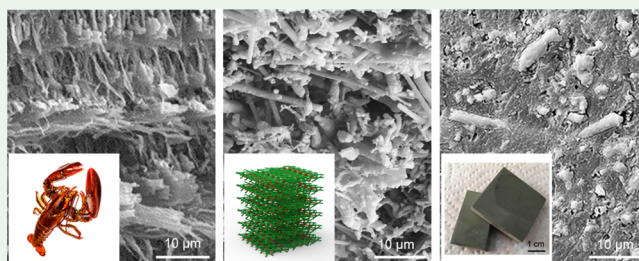
[§]State Key Laboratory of Advanced Non-ferrous Materials, Lanzhou University of Technology, Lanzhou 730050, China

^{||}Department of Materials Science and Engineering, University of California Berkeley, Berkeley, California 94720, United States

Supporting Information

ABSTRACT: Crustacean exoskeletons demonstrate exceptional mechanical efficiency owing to their intricate architectures. However, the translation of their underlying structural design to man-made material systems represents a challenge. Here we report the “top-down” fabrication using freeze casting of silicon carbide hybrid composites which contain a compliant phase and mimic the structure of crustacean exoskeletons. The composites display laminated interwoven nanoarchitectures that replicate the main structural design motifs of crustacean exoskeletons, i.e., the laminated arrangement, varying in-plane orientations, and three-dimensional interconnection by abundant nano-interconnectivities of constituents. The laminated interwoven nanoarchitectures create an enhancement in several extrinsic toughening mechanisms, specifically crack deflection/twisting and uncracked-ligament bridging, which results in increasing fracture resistance with crack extension, i.e., rising R-curve behavior, and outstanding strength–toughness combinations, especially as compared to layered composites. Our approach is feasible for the efficient fabrication of bioinspired composites mimicking crustacean exoskeletons and demonstrates a promising potential for the development of new synthetic lightweight structural materials with exceptional combinations of mechanical properties.

KEYWORDS: *bioinspiration, hybrid composite, architecture, fracture toughness, crustacean exoskeleton*



1. INTRODUCTION

Natural materials are distinguished by an exceptional efficiency in developing combinations of outstanding mechanical properties, e.g., strength and fracture toughness, using a limited selection of constituents.^{1–3} These materials, in particular their underlying design principles extracted from the perspective of materials science, offer a source of inspiration for the development of new, high-performance materials in man-made systems.^{4–8} In this regard, among the diversity of natural materials, crustacean exoskeletons are characterized by a unique multifunctionality to fulfill stringent mechanical tasks by providing not only mechanical support and load-bearing capability but also an effective protection to the body against environment and predators; some types of exoskeletons even function as a weapon for fighting or feeding.⁹ It has been well established that the mechanical performance of crustacean exoskeletons originates principally from their intricate structural design.^{10–22} A basic motif of such design is the nanoscale mineralized chitin-protein fibers that are arranged in a laminated fashion with their in-plane orientations continu-

ously varying within the laminates, frequently forming twisted plywood or Bouligand-type architectures.^{11–13} This endows the crustacean exoskeletons with potent toughening mechanisms, specifically crack deflection and twisting along the interfaces of constituents, thus greatly enhancing their fracture toughness and energy-dissipation capability.²¹ Additionally, the mechanical properties of these natural materials demonstrate good macroscopic isotropy in two dimensions owing to the variations of the orientations of constituents.²²

The ingenious design of crustacean exoskeletons offers an excellent paradigm for biomimicry; however, its implementation into man-made systems still remains a challenge with success limited to but a few examples in practice.^{23–30} The main difficulty lies in the realization of (i) the laminated arrangement of constituents and (ii) the variations of their in-plane orientations. One conventional approach is to lay up

Received: January 18, 2019

Accepted: January 23, 2019

Published: January 23, 2019

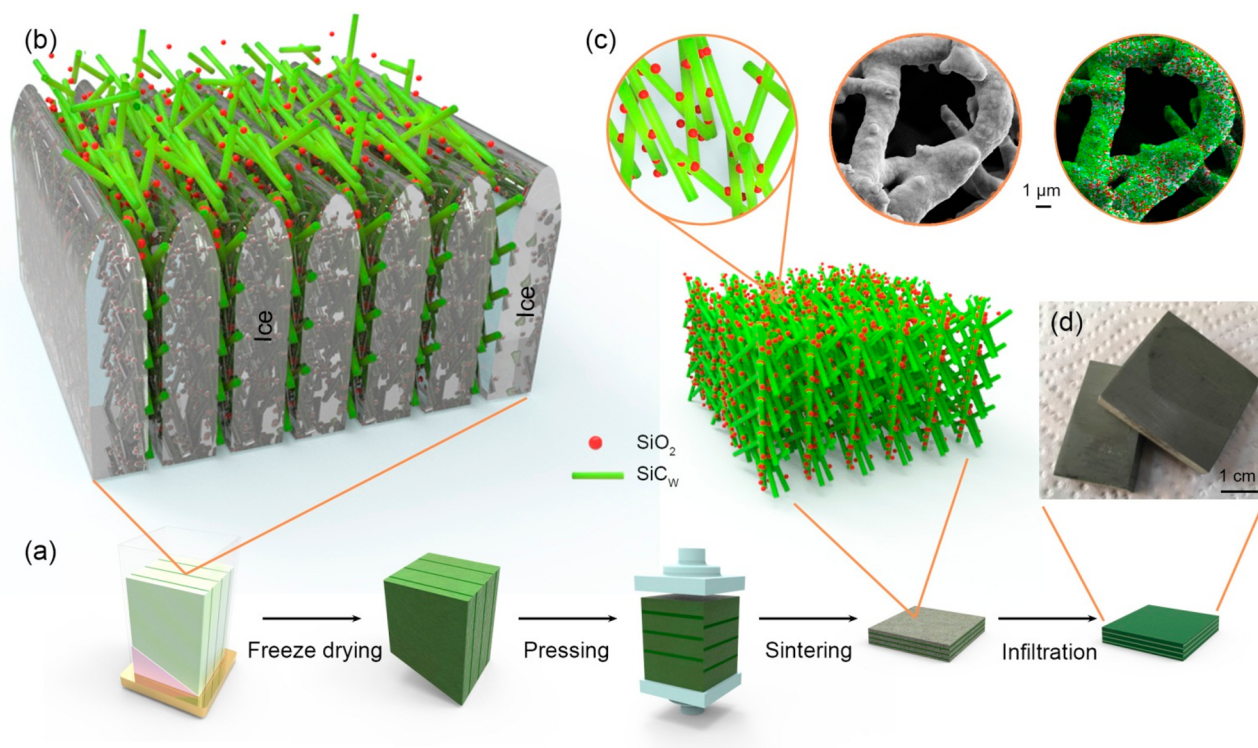


Figure 1. Formation process of bioinspired hybrid composites with laminated interwoven nanoarchitectures. (a) Schematic illustration of the processing route for the fabrication of bioinspired silicon carbide–PMMA composites. (b) Illustration of the micromechanism near the ice front during the freeze casting process. (c) Illustration and SEM micrograph with energy dispersive spectroscopy imaging of the sintered scaffold. (d) Image of the macroscopic morphology of hybrid composites after infiltration.

composite plies, which contain unidirectionally aligned reinforcements but are rotated by different angles, followed by consolidation.^{22,24} This enables a precise control of the fiber orientations but generally results in a dimensionally coarse composite microstructure (typically on the length-scale of tens to hundreds of micrometers). Additive manufacturing, e.g., 3-D printing, allows for the construction of complex architectures in materials, thus providing a novel means for the fabrication of materials mimicking crustacean exoskeletons. The orientations of constituents with large aspect ratios can be readily regulated during processing by applying shear force or using magnetic or electric fields.^{5,8,25–29} However, this method is complicated by the necessity of surface modification of the constituents to make them magnetic- or electric-responsive using specific additives and an accurate modulation of applied fields in the process of manufacturing. Indeed, such “bottom-up” approaches, including layer-by-layer assembly, are generally restricted by a limited efficiency in fabricating bulk materials. Moreover, the materials reported to date that mimic crustacean exoskeletons using such methods invariably demonstrate poor interconnectivity both between the laminates and between the constituents within laminates. As such, these synthetic materials become susceptible to delamination and debonding of the fibers, which compromises their mechanical properties and can result in premature failure. In contrast, in natural crustacean exoskeletons, the adjacent fibers and laminates are interconnected or stitched together by abundant trans-lamellar tubules.^{10–14} Such interconnectivity represents an additional structural feature to be replicated in man-made materials mimicking crustacean exoskeletons.

2. RESULTS AND DISCUSSION

2.1. Structural Characteristics. Figure 1 illustrates the formation process of the bioinspired hybrid composites, which comprise freeze-cast silicon carbide containing a poly(methyl methacrylate) (PMMA) compliant phase and exhibit laminated interwoven nanoarchitectures that replicate the structural design of crustacean exoskeletons (as described in the [Materials and Methods](#) section). During the freezing process, a horizontal temperature gradient is generated in the slurry because of a polydimethylsiloxane (PDMS) wedge placed between the slurry and the coldfinger, in addition to the vertical temperature gradient created by the coldfinger. As such, the ice crystals nucleated at the bottom of the wedge preferentially grow in two directions, i.e., vertically from the bottom to the top away from the coldfinger and horizontally along the wedge. This enables the ice crystals to grow into a long-range aligned lamellar structure.^{31,32} In this process, the nanoscale mineral particles and additives mixed in the slurry are gradually expelled into the microspace between growing ice crystals.^{33,34} In particular, the encapsulating force exerted by the moving ice front triggers the self-assembly of the silicon carbide whiskers, which possesses a large aspect ratio and anisotropy, by realigning their long axes preferentially parallel to the profile of growing ice crystals (Figure 1b).^{23,35} This leads to the laminated arrangement of whiskers with their in-plane orientations randomly distributed within the laminates. The subsequent sublimation of the ice via freeze-drying results in a scaffold with aligned pores replicating the ice crystals.

The pressing treatment along the orthogonal direction helps densify the scaffold to improve the mineral content in the composites. This plays an additional role in enhancing the

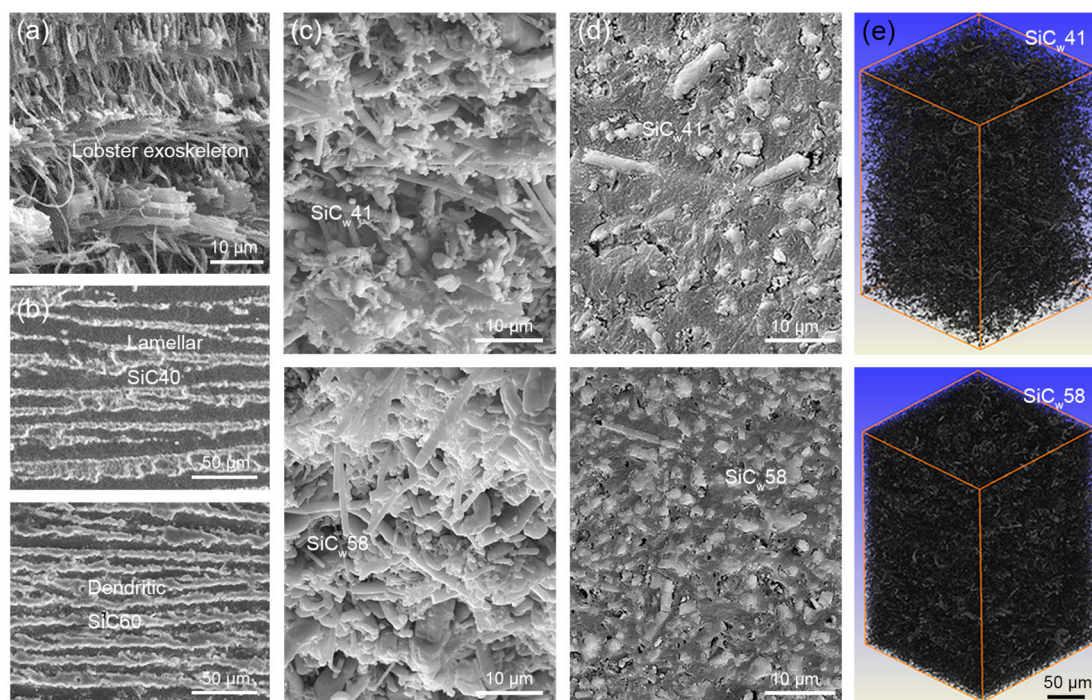


Figure 2. Structure of sintered scaffolds and infiltrated composites compared to lobster exoskeleton and layered composites. (a) Structure of the exoskeleton of a lobster *Homarus americanus* [Adapted with permission from ref 10. Copyright 2005 Elsevier]. (b) Structures of layered composites with lamellar and dendritic morphologies [Adapted with permission from ref 42. Copyright 2015 Elsevier]. (c) SEM micrographs of the sintered scaffolds subjected to single and twice pressing treatment before sintering. (d) SEM micrographs of the polished cross sections of infiltrated composites with different mineral contents. SiC_W41 and SiC_W58 refer respectively to materials with mineral contents of 41 and 58 vol %. (e) XRT volume renderings of the composites with signal filtered for the silicon carbide reinforcements, i.e., the PMMA matrix is transparent.

microstructural ordering of the composites by decreasing the out-of-plane misalignment of silicon carbide whiskers.³⁶ In the sintering process, at a lower temperature than that used to sinter the silicon carbide, the scaffold is partially sintered with the silicon carbide whiskers interconnected by the doped silica nanoparticles (Figure 1c), resulting in a good integrity of the scaffold through the formation of abundant nanointerconnectivities in three-dimensional space. Additionally, this treatment produces mineral nanoasperities on the surface of whiskers, reminiscent of the nanoscale features of the mineral platelets in nacre.^{37–39} Such nanoasperities serve to promote bonding strength between the mineral and polymeric phases by increasing their interfacial roughness in biological and bioinspired materials.^{37–40} In the present composites, the interfaces can be additionally strengthened by grafting the scaffold with γ -MPS which creates covalent bonds between mineral reinforcements and PMMA matrix.^{41,42}

The structures of sintered scaffolds and infiltrated composites are compared to the exoskeleton of a lobster *Homarus americanus*¹⁰ and the layered silicon carbide–PMMA composites with lamellar and dendritic morphologies⁴² in Figure 2. The lobster exoskeleton, shown in Figure 2a, demonstrates a laminated structure with in-plane orientations of the nanoscale mineralized chitin-protein fibers with diameter of 50–250 nm continuously varying between adjacent laminates. Abundant trans-lamellar tubules are present in the exoskeleton to connect these laminates, leading to sound interconnections. The mineral contents of crustacean exoskeletons differ markedly among varying species, e.g., ~50–73 wt % for the lobster *Homarus americanus* and ~77–89 wt % for the crab *Cancer pagurus*.^{19,43} Additionally, the

mineral contents vary significantly among different locations within the exoskeletons even for the same species. In the case of the present lobster exoskeleton, the mineral content increases from the carapace (50 wt %) to the claw (61 wt %) to the finger (73 wt %).⁴³ A series of nacrelite composites with layered structures have been fabricated in the silicon carbide–PMMA system with mineral contents ranging from 40 to 60 vol % using the freeze-casting technique.⁴² Such composites present an increasing density of nanointerconnectivity and display a transition from lamellar morphology to dendritic morphology with increasing mineral content (Figure 2b). As a comparison, the silicon carbide whiskers in the present scaffolds can be seen to be arranged in a laminated fashion, as shown in Figure 2c; their long axes are preferentially aligned within the laminates but are randomly oriented in two dimensions. These whiskers are interconnected, staggered, and intersected with each other in three-dimensional space, forming continuous interwoven mineral networks. Hybrid composites strengthened by such networks were generated by filling the porosity with PMMA (Figure 2d). X-ray tomography (XRT) volume renderings clearly visualize the three-dimensional laminated interwoven nanoarchitectures of silicon carbide whiskers in these composites (Figure 2e).

The structures of the present hybrid composites resemble to a large extent that of the lobster exoskeleton. In particular, we have translated the major design motifs of crustacean exoskeletons into synthetic composites, specifically, the laminated arrangement and varying in-plane orientations of the constituents together with three-dimensional nanointerconnections between them. It is noted that many crustacean exoskeletons in nature demonstrate some kind of structural

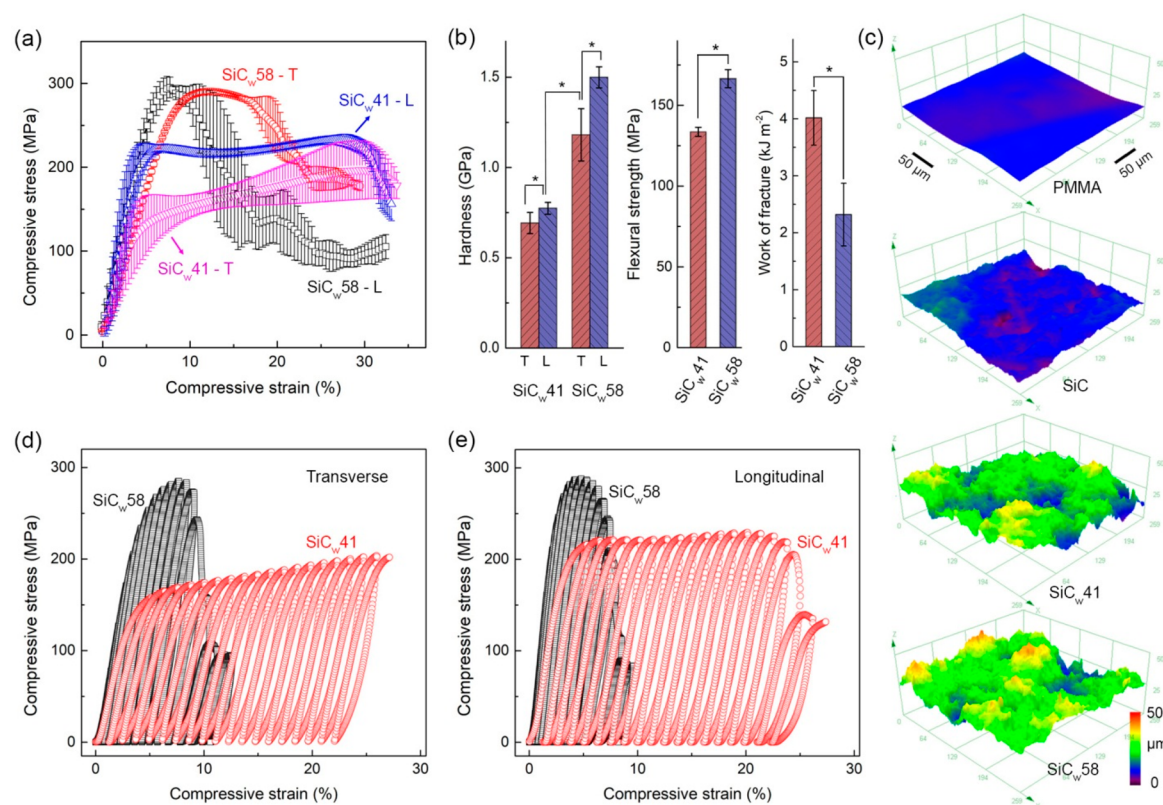


Figure 3. Mechanical properties of bioinspired hybrid composites mimicking crustacean exoskeletons. (a) Compressive stress–strain curves of the composites along different orientations. T and L refer to the transverse and longitudinal orientations of composites. (b) Comparison of hardness, flexural strength, and work of fracture between composites with different mineral contents. Asterisks indicate statistically significant differences. (c) Tomography images of the fracture surfaces of bent composites compared to monolithic PMMA and silicon carbide. (d, e) Cyclic compressive stress–strain curves of composites along (d) transverse and (e) longitudinal orientations.

regularity with their mineralized chitin-protein fibers aligned in a similar orientation within a single lamella.^{10–14} The lamellae may even display certain periodicity in their arrangement, sometimes forming the so-called Bouligand-type structure.^{11,12} In spite of the lack of a rigid replication of such characteristics *per se*, several underlying designs that essentially endow crustacean exoskeletons with exceptional biomechanical functionality have been successfully implemented in the present composites. This enables the activation of the principal mechanisms used by nature in the composites toward enhanced mechanical properties—it is through such an optimizing strategy in which the composites mimic the crustacean exoskeletons.

The porosity in the scaffolds can be adjusted by pressing the green bodies before sintering, leading to varying mineral contents in the resultant composites. Even lower mineral contents can be obtained without pressing and controlled by adjusting the concentration of mineral constituents in the slurry. The mineral contents of the present composites subjected to single and double pressing treatments were determined to be 41 vol % and 58 vol % (equivalent to ~65% and 79% by weight), respectively. Such mineral contents are comparable to those of the natural lobster exoskeleton and the synthetic silicon carbide–PMMA composites with layered structures.^{19,42,43} Note here that the appearance of tiny pits in the scanning electron microscopy (SEM) images (Figure 2d) is an artifact caused by the pull-out of silicon carbide whiskers from the polymeric matrix during the polishing process of samples. No pores or apparent agglomeration of minerals can

be detected in the XRT images (Figure 2e), indicating a complete infiltration and good structural uniformity of the composites.

2.2. Mechanical Properties. The compressive stress–strain curves shown in Figure 3a demonstrate the capability of the composites to undergo large strains (exceeding 10%) prior to fracture. In particular, the composites with lower mineral content (41 vol %) display significant stable plastic deformation of over 20% without apparent stress reduction. Both composites are much more ductile than monolithic silicon carbide which virtually has no plasticity. The compressive strength, hardness, and flexural strength are markedly improved with the increase of mineral content from 41 to 58 vol % (Figure 3b). The work of fracture in bending, represented using the area under load–displacement curve divided by the area of the load-bearing cross-section of samples, presents an opposite varying trend with the composite with lower mineral content ~73% tougher than that with higher mineral content (Figure S1 in the Supporting Information for flexural stress–displacement curves). Moreover, the composites display strong mechanical anisotropy in hardness with the longitudinal orientation, i.e., the in-plane orientation of laminates, being significantly harder than the transverse orientation, i.e., the orientation orthogonal to laminates. Specifically, the hardness in the longitudinal orientation is ~12% and 27%, respectively, higher than the transverse orientation in composites with mineral contents of 41 and 58 vol % (hereinafter referred to as SiCw41 and SiCw58, respectively). The compressive strength demonstrates

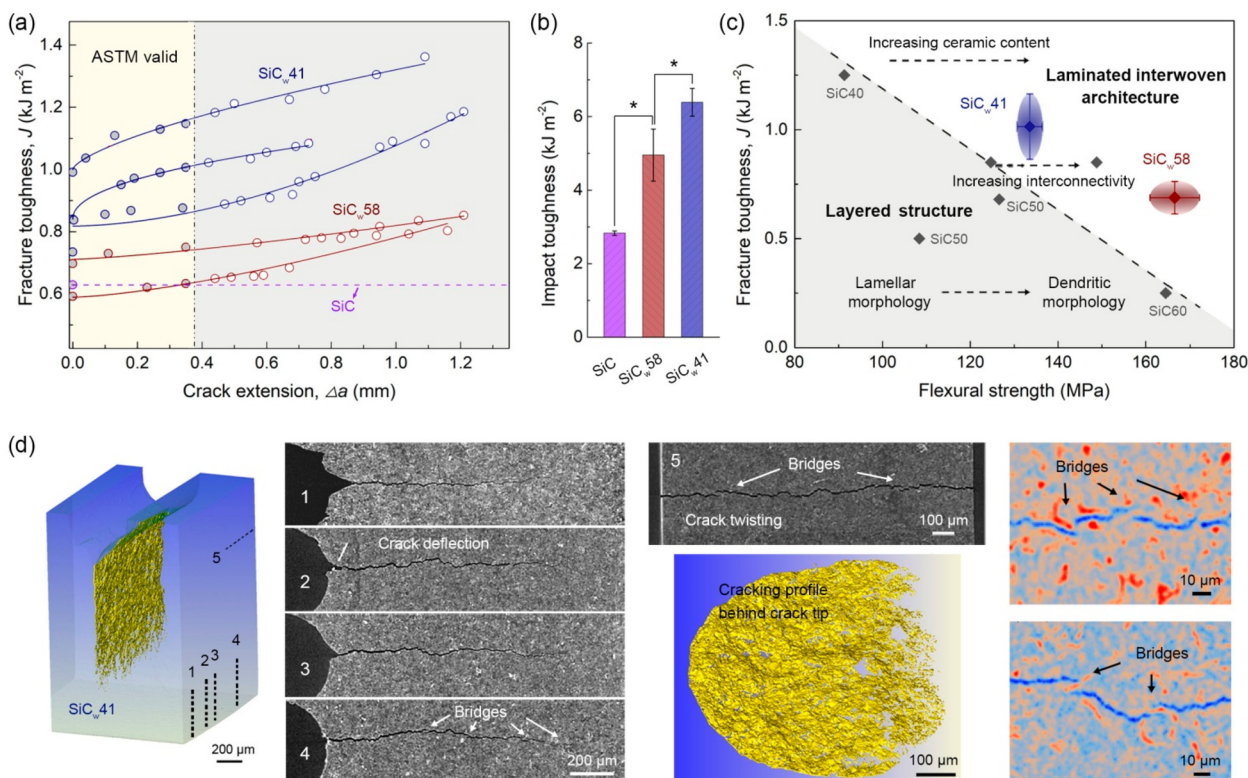


Figure 4. Damage tolerance and toughening mechanisms of bioinspired hybrid composites with laminated interwoven nanoarchitectures. (a) Crack-resistance curves (R-curves) showing the fracture toughness of composites in terms of J as a function of crack extension. (b) Impact toughness of composites with different mineral contents compared to monolithic silicon carbide. (c) Comparison of the combinations of flexural strength and fracture toughness of silicon carbide–PMMA composites with laminated interwoven nanoarchitectures and layered structures.⁴² The mineral contents are indicated in the figure. (d) XRT images of crack propagation from a sharpened notch tip showing multiple toughening mechanisms in the composites. Slices 1–4 are parallel to the crack growth direction. Slice 5 is perpendicular to the crack growth direction.

a similar anisotropy in the SiCw41 composite; nevertheless, such a trend is insignificant for the SiCw58 composite (the decreased anisotropy may result from the presence of multiple randomly distributed nanointerconnections between the minerals as the compressive strength is largely associated with the failure of the scaffold of mineral reinforcements⁴⁴).

Tomography imaging reveals a distinct unevenness on the fracture surfaces of bent composites, as shown in Figure 3c, which contrasts to the smooth surfaces of monolithic PMMA or silicon carbide. This is presumed to result from the pull-out of whiskers or whisker bundles from the polymeric matrix and the shear deformation between laminates and acts to dissipate more mechanical energy at fracture. In addition, the cyclic compressive stress–strain curves of composites are characterized by remarkable hysteresis loops for both orientations (Figure 3d and e). This suggests a distinct capability for effective energy consumption by viscoelasticity during the loading–unloading cycles. The viscoelasticity is more prominent for the composite with lower mineral content (i.e., SiCw41) which exhibits stable hysteresis loops and large plastic deformation (Figure S2 in the Supporting Information for the amount of energy dissipation). Additionally, such composites demonstrate more efficient energy consumption for the longitudinal orientation, as compared to that in the transverse orientation.

The fracture toughness evaluation combined with *in situ* measurement of crack length by SEM observation reveals a rising crack-resistance (R-curve) behavior of the composites where the crack-growth toughness increases with crack

extension (Figure 4a). Such stable crack growth contrasts to the catastrophic fracture of monolithic silicon carbide. Indeed, the main toughening function of compliant phase in ceramics is to stabilize slow crack growth to avoid sudden fracture.¹ The composites with lower mineral content exhibit an improved crack-growth toughness in the form of a steeper R-curve and hence a higher tolerance for stable crack growth before unstable fracture ensues. According to the ASTM standards (E1820-13),⁴⁵ the maximum fracture toughness in terms of the J -integral of a specimen is limited by the smaller of $b\sigma_y/10$ or $B\sigma_y/10$ with σ_y being the effective yield strength; also, the maximum crack extension is limited by $0.25b$. By applying such criteria, the critical valid fracture toughness was determined to be 1.0 ± 0.1 and 0.69 ± 0.07 kJ m^{-2} , respectively, for the SiCw41 and SiCw58 composites, which is roughly 61% and 10% higher than that of monolithic silicon carbide. The impact toughness presents a similar varying trend with mineral content as the fracture toughness (Figure 4b). The SiCw41 and SiCw58 composites are, respectively, about 2.3 and 1.7 times tougher than monolithic silicon carbide under dynamic loading conditions.

It has been well-established that the layered arrangement of inorganic and organic constituents at the nano- to micro-length-scales in composites reminiscent of the designs in biological materials like nacre, generate several extrinsic toughening mechanisms, such as uncracked-ligament bridging, pull-out of crack bridges, and crack deflection along the interfaces.^{4,11,46–48} This may lead to a significant enhancement in the fracture toughness without necessarily decreasing

strength, thus endowing the composites with superior strength–toughness combinations as compared to a simple mixture of constituents. Silicon carbide has been widely used as a reinforcement phase in strengthening the polymeric matrix in silicon carbide–polymer composite system.^{25,49–52} The current hybrid materials are stronger than most of such polymer-based composites because of their higher mineral content and enhanced nanointerconnection between the reinforcements. In addition, the mechanical properties of the nacre-like silicon carbide–PMMA composites with layered structures have been investigated and correlated to their microstructural characteristics.⁴² These composites display a general varying trend of increasing strength and decreasing fracture toughness as the mineral content increases. Their mechanical properties are additionally associated with the composite architecture and can be improved by increasing the nanointerconnectivity between lamellae. A direct comparison shows that the present composites exhibit markedly higher fracture toughness than the layered ones at an equivalent level of strength (Figure 4c). Comparable strength–toughness combinations cannot be readily generated in layered composites without the presence of distinct interconnecting regions that can bridge the mineral lamellae.⁴² This demonstrates the marked efficiency of laminated interwoven nanoarchitectures in toughening natural composites, specifically as compared to the layered structures with lamellar or dendritic morphologies.

Reconstructed tomography imaging of crack propagation from a sharpened notch tip, shown in Figure 4d, reveals the existence of multiple mechanisms in the composites that serve to resist the growth of cracks. A prime feature is the torturous nature of the cracking profile at the microscale. On the one hand, the crack displays a wavy path along its growth direction, resulting primarily from the laminated arrangement of constituents. Such in-plane crack deflection helps shield the crack tip from applied stress and is widely utilized as an effective toughening strategy in biological and bioinspired material-systems, especially those with layered structures.^{4,41,42,48} On the other hand, the inconsistency between the crack traces at differing longitudinal cross sections (slices 1–4) indicates apparent unevenness of cracking profile perpendicular to the growth direction. Such a characteristic, termed out-of-plane crack twisting to differentiate from the above-mentioned crack deflection, is clearly visualized in the through-thickness cross-section of XRT images (slice 5). Significant crack twisting has rarely been reported in layered composites in the case of cross-layer cracking, i.e., the crack propagates along the orthogonal direction of layered structure.^{41,42} This is due to the lack of microstructural heterogeneity in the composites along the out-of-plane directions. The enhanced crack twisting in the present composites is closely associated with the interwoven nanoarchitectures and the varying orientations of whiskers. It acts to increase the spatial complexity of the cracking profile and markedly strengthen the crack-tip shielding effect, thus allowing for more efficient toughening as compared to simple (in-plane) crack deflection.⁴⁸

Additionally, crack bridging is evident in our composites with the crack bridged by numerous nano- to micro-sized uncracked ligaments. In particular, the crack wake directly behind the crack tip remains largely intact and connected, as shown in the reconstructed images shown in Figure 4d. The fibrous nature of constituents and their good interconnection

are responsible for the formation of numerous crack bridges; such bridges serve to inhibit the crack opening and carry load which would otherwise be used to promote crack growth. Their fracture and subsequent pull-out from the polymeric matrix additionally dissipate mechanical energy.⁵³ Therefore, the outstanding mechanical properties of the present composites, in particular compared to those with layered structures, originate essentially from potent extrinsic toughening, principally in the form of enhanced crack twisting and uncracked-ligament bridging, which is generated by the implementation of the design principles derived from crustacean exoskeletons.

3. CONCLUSIONS

We have fabricated new silicon carbide hybrid composites containing a compliant phase with bioinspired laminated interwoven nanoarchitectures mimicking crustacean exoskeletons primarily using a freeze-casting technique. The composites successfully replicate several basic design principles extracted from crustacean exoskeletons, i.e., the laminated structural arrangement, varying orientations of constituents, and three-dimensional nanointerconnections. This endows them with outstanding combinations of strength and fracture toughness for the silicon carbide–polymer material system, specifically as compared to the layered composites with lamellar or dendritic structural morphologies that mimic nacre. Our bioinspired composites exhibit improved toughness under both quasi-static and impact loading with rising R-curve behavior. In particular, the laminated interwoven nanoarchitectures demonstrate a remarkable toughening efficiency, especially as compared to the layered structures, by enhancing the extrinsic toughening primarily attained from in-plane crack deflection, out-of-plane crack twisting, and uncracked-ligament bridging. Our study offers a promising approach for an efficient fabrication of bulk hybrid materials that mimic crustacean exoskeletons using a “top-down” approach and for the preferential alignment of other constituents with large aspect ratios in composites. The enhanced combinations of strength and fracture toughness are critical for the structural applications of lightweight materials. We anticipate that the current composites may be potentially used to partially replace PMMA or other polymers in areas where higher strength is needed, or to partially replace ceramic materials where improved toughness is preferred. Additionally, the current design motifs inspired by crustacean exoskeletons may be further employed to develop new nanocomposites with exceptional mechanical properties, especially in toughening materials that are inherently brittle.

4. MATERIALS AND METHODS

4.1. Composite Fabrication. The processing route used to fabricate the nanocomposites is illustrated in Figure 1. An aqueous suspension was prepared by dispersing in deionized water 11.2 wt % silicon carbide whiskers (in β -crystalline form, Ksfuns Co., China), with diameter of 0.1–1 μm and length of 5–10 μm , 0.4 wt % silica nanopowders (Huisheng New Materials Co., China), with diameter of ~ 15 nm, and 0.2 wt % Darvan CN dispersing agent (R.T. Vanderbilt Co., Norwalk, CT). The viscosity of the slurry was adjusted by adding 1.6 wt % hydroxypropyl methylcellulose (Meryer Co., China), 3.9 wt % poly(vinyl alcohol) (molecular weight of 84–89 kDa, Meryer Co., China), and 3.9 wt % sucrose to avoid gravitational sedimentation. These organics also serve as a binder of mineral powders after removal of the water. The mixture was ball-milled for 24 h, deaired by adding one drop of defoamer (XP-M-120, Huaxing Co., China), and then

ball-milled for another 2 h. The suspension was poured into square plastic mold in dimension of 30 mm × 30 mm × 70 mm containing a PDMS wedge with a slope angle of 25° at the bottom. The wedge functions to create a horizontal temperature gradient from its thinner end to thicker end during freezing, thus allowing for the generation of long-range aligned lamellar structure.^{23,31} The mold was placed on a copper coldfinger of which the other end was immersed in liquid nitrogen. The average cooling rate of the slurry was estimated to be in the range of 10–20 °C/min based on its freezing front velocity.^{32,54}

Frozen samples were dried in vacuum below 5 Pa for over 48 h using a Scientz-10ND freeze drier (Scientz Biotechnology Co., China). These samples were subsequently pressed at 65 MPa along the orthogonal direction of the lamellar structure at ~130 °C, the softening temperature range of the organics. The green bodies were heat-treated at 500 °C for 2.5 h in air to burn out the organics and then sintered at 1100 °C for 2 h. This sintering temperature was chosen to limit oxidation of the silicon carbide while still allowing the nanometer-sized silica to be sintered to form nanointerconnections between the silicon carbide whiskers.^{23,55} Some of the green bodies were additionally densified before sintering by subjecting them to a pressure of 65 MPa along the orthogonal direction to generate a higher mineral content in the final composites. The as-sintered scaffolds were grafted with γ -methacryloxypropyltrimethoxysilane (γ -MPS, Chiyechem Co., China) by immersing in a methanol–water solution (methanol/water = 9/1 by weight) containing 20 wt % γ -MPS for 24 h. The pH of the solution was adjusted to 4 by adding acetic acid before immersing. Such surface modification helps strengthen the interfacial adhesion between the mineral and polymeric phases after infiltration.^{41,42} The grafted scaffolds were dried at 50 °C for 10 h and then infiltrated with methyl methacrylate (Jihua Co., China) containing 0.5 wt % 2,2-azobis(isobutyronitrile) as an initiator under a negative pressure below 80 kPa. The samples were heat-treated at 40 °C for 40 h and additionally at 90 °C for another 2 h to allow for a full polymerization of the monomers to form the PMMA matrix in the composites.

4.2. Characterization. Scanning electron microscopy imaging was performed on the sintered scaffolds and polished cross sections of infiltrated composites using a LEO Supra-55 field-emission scanning electron microscope operating at an accelerating voltage of 20 kV. The samples were sputtered-coated with a film of gold before imaging. Image analysis was conducted using the ImageJ software to quantify the content of the mineral phase.⁵⁶ Energy dispersive spectroscopy measurement was carried out using an Oxford Model 7426 spectrometer. X-ray tomography imaging was performed using an Xradia VersaXRM-500 3D X-ray microscope operating at an accelerating voltage of 80 kV. Images were processed and analyzed using the Avizo Fire 7.1 software.⁵⁷

Hardness measurements were conducted on the polished profiles of composites using an MH-5L Vickers hardness tester with a load of 1 kg and dwell time of 15 s. Uniaxial compression tests were performed on rectangular samples with a cross-section of 2 mm × 2 mm and height of 4 mm at a strain rate of 10⁻³ s⁻¹ using an Instron 5982 testing system equipped with an Instron 2580 static load cell and an Instron 2601-92 linear variable differential transformer deflection sensor. For cyclic compression, samples with the same dimensions as those used for uniaxial compression were loaded and unloaded repeatedly at a constant strain rate of 10⁻³ s⁻¹ to reach a constant increase of strain of ~1% at each cycle until failure. Flexural tests were performed on beam samples cut and polished to a cross-section of 2 mm × 1.5 mm with a loading span of 20 mm, in accordance with ASTM Standard C1161-13.^{30,58} The tests were carried out at a displacement rate of 0.06 mm min⁻¹ using an Instron E1000 testing system with an Instron 2527-302 load cell and an accessional displacement sensor. After testing, the fracture surfaces of samples were examined using an Olympus LEXT OLS-4000 3D measuring laser microscope. Impact tests were conducted on samples, with the same dimensions as used for the flexure tests, using a Zwick HITSOP pendulum impact testing machine with impact energy of 2 J. The bending and impact mechanical properties of composites were measured as a function of applied load along the orthogonal direction

of the laminates. This is the most common loading direction for static or impact bending in terms of the application of laminated composites in both natural (e.g., crustacean exoskeletons) and man-made systems. At least four samples were tested for each type of mechanical test. The differences in mechanical properties were tested using two-tailed Student's *t*-test with values *P* < 0.05 being considered statistically significant.

Single-edge notched bend SE(B) tests were performed on samples cut and polished to a width (*W*) of 3 mm and thickness (*B*) of 1.5 mm with a loading span of 12.5 mm. The samples were side-notched to a depth of ~1.5 mm perpendicular to the plane of whisker alignment using a low-speed diamond saw with the notch root sharpened by a razor blade, in general accordance with ASTM designation D5045-99.^{30,42,59} In this configuration, crack propagation was aligned to be nominally perpendicular to the laminates, i.e., in the direction that toughening from fiber pull-out and crack bridging is most active⁵³. Testing was conducted at a displacement rate of 4 × 10⁻³ mm min⁻¹ on a JEOL MicroTest stage inside the chamber of a JEOL JSM-6510 scanning electron microscope. Nonlinear-elastic fracture mechanics methods were employed to evaluate the fracture resistance of the composites in terms of the *J*-integral as a function of crack extension, Δa . *J* is defined as the rate of change in potential energy per unit increase in crack area for a nonlinear elastic solid; the critical value of *J*, e.g., at crack initiation or for crack growth, can be equated to the fracture toughness of the material. The *J*-integral, corresponding to each crack length, *a*, which was measured *in situ* in the SEM, is given by $J = (1.9A_{\text{tot}})/Bb$, where A_{tot} is the total area under the load–displacement curve and *b* is the uncracked ligament width (i.e., $b = W - a$). More details about the analysis can be found in refs 41 and 42.

■ ASSOCIATED CONTENT

📄 Supporting Information

The Supporting Information is available free of charge on the ACS Publications website at DOI: 10.1021/acsanm.9b00063.

Compressive strength, flexural stress–displacement curves, and energy dissipation during the loading–unloading cycles for cyclic compression of the hybrid composites with laminated interwoven nanoarchitectures inspired by the crustacean exoskeleton (PDF)

■ AUTHOR INFORMATION

Corresponding Authors

*Tel.: +86-24-8397-0116. Fax: +86-24-8397-0116. E-mail address: zengqianliu@imr.ac.cn (Z.L.).

*Tel.: +86-24-8397-1043. Fax: +86-24-2389-1320. E-mail address: zhfhzhang@imr.ac.cn (Z.Z.).

*Tel.: +1-510-409-1779. Fax: +1-510-643-5792. E-mail address: roritchie@lbl.gov (R.O.R.).

ORCID

Robert O. Ritchie: 0000-0002-0501-6998

Notes

The authors declare no competing financial interest.

■ ACKNOWLEDGMENTS

The authors are grateful for the financial support by the National Natural Science Foundation of China under grant nos. 51871216 and 51331007 (for Z.L. and Z.Z.) and from the Multi-University Research Initiative under grant no. AFOSR-FA9550-15-1-0009 from the Air Force Office of Scientific Research to the University of California Riverside, specifically through a subcontract to the University of California Berkeley (for Z.L. and R.O.R.).

REFERENCES

- (1) Wegst, U. G. K.; Bai, H.; Saiz, E.; Tomsia, A. P.; Ritchie, R. O. Bioinspired Structural Materials. *Nat. Mater.* **2015**, *14*, 23–36.
- (2) Meyers, M. A.; Chen, P. Y.; Lin, A. Y. M.; Seki, Y. Biological Materials: Structure and Mechanical Properties. *Prog. Mater. Sci.* **2008**, *53*, 1–206.
- (3) Jackson, A. P.; Vincent, J. F. V.; Turner, R. M. The Mechanical Design of Nacre. *Proc. R. Soc. London B* **1988**, *234*, 415–440.
- (4) Munch, E.; Launey, M. E.; Alsem, D. H.; Saiz, E.; Tomsia, A. P.; Ritchie, R. O. Tough, Bio-Inspired Hybrid Materials. *Science* **2008**, *322*, 1516–1520.
- (5) Studart, A. R. Towards High-Performance Bioinspired Composites. *Adv. Mater.* **2012**, *24*, 5024–5044.
- (6) Liu, Z. Q.; Zhu, Y. K.; Jiao, D.; Weng, Z. Y.; Zhang, Z. F.; Ritchie, R. O. Enhanced Protective Role in Materials with Gradient Structural Orientations: Lessons from Nature. *Acta Biomater.* **2016**, *44*, 31–40.
- (7) Bonderer, L. J.; Studart, A. R.; Gauckler, L. J. Bioinspired Design and Assembly of Platelet Reinforced Polymer Films. *Science* **2008**, *319*, 1069–1073.
- (8) Studart, A. R. Additive Manufacturing of Biologically-Inspired Materials. *Chem. Soc. Rev.* **2016**, *45*, 359–376.
- (9) Liu, Z. Q.; Zhang, Z. F.; Ritchie, R. O. On the Materials Science of Nature's Arms Race. *Adv. Mater.* **2018**, *30*, 1705220.
- (10) Raabe, D.; Sachs, C.; Romano, P. The Crustacean Exoskeleton as an Example of a Structurally and Mechanically Graded Biological Nanocomposite Material. *Acta Mater.* **2005**, *53*, 4281–4292.
- (11) Suksangpanya, N.; Yaraghi, N. A.; Pipes, R. B.; Kisailus, D.; Zavattieri, P. Crack Twisting and Toughening Strategies in Bouligand Architectures. *Int. J. Solids Struct.* **2018**, *150*, 83–106.
- (12) Suksangpanya, N.; Yaraghi, N. A.; Kisailus, D.; Zavattieri, P. Twisting Cracks in Bouligand Structures. *J. Mech. Behav. Biomed. Mater.* **2017**, *76*, 38–57.
- (13) Guarán-Zapata, N.; Gomez, J.; Yaraghi, N.; Kisailus, D.; Zavattieri, P. D. Shear Wave Filtering in Naturally-Occurring Bouligand Structures. *Acta Biomater.* **2015**, *23*, 11–20.
- (14) Raabe, D.; Romano, P.; Sachs, C.; Fabritius, H.; Al-Sawalmih, A.; Yi, S. B.; Servos, G.; Hartwig, H. G. Microstructure and Crystallographic Texture of the Chitin-Protein Network in the Biological Composite Material of the Exoskeleton of the Lobster. *Mater. Sci. Eng., A* **2006**, *421*, 143–153.
- (15) Liu, Z. Q.; Meyers, M. A.; Zhang, Z. F.; Ritchie, R. O. Functional Gradients and Heterogeneities in Biological Materials: Design Principles, Functions, and Bioinspired Applications. *Prog. Mater. Sci.* **2017**, *88*, 467–498.
- (16) Nikolov, S.; Fabritius, H.; Petrov, M.; Friák, M.; Lymperakis, L.; Sachs, C.; Raabe, D.; Neugebauer, J. Robustness and Optimal Use of Design Principles of Arthropod Exoskeletons Studied by Ab Initio-Based Multiscale Simulations. *J. Mech. Behav. Biomed. Mater.* **2011**, *4*, 129–145.
- (17) Fabritius, H. O.; Sachs, C.; Triguero, P. R.; Raabe, D. Influence of Structural Principles on the Mechanics of a Biological Fiber-Based Composite Material with Hierarchical Organization: The Exoskeleton of the Lobster *Homarus Americanus*. *Adv. Mater.* **2009**, *21*, 391–400.
- (18) Weaver, J. C.; Milliron, G. W.; Miserez, A.; Evans-Lutterodt, K.; Herrera, S.; Gallana, I.; Mershon, W. J.; Swanson, B.; Zavattieri, P.; DiMasi, E.; Kisailus, D. The Stomatopod Dactyl Club: A Formidable Damage-Tolerant Biological Hammer. *Science* **2012**, *336*, 1275–1280.
- (19) Chen, P. Y.; Lin, A. Y. M.; McKittrick, J.; Meyers, M. A. Structure and Mechanical Properties of Crab Exoskeletons. *Acta Biomater.* **2008**, *4*, 587–596.
- (20) Meyers, M. A.; Lin, A. Y. M.; Seki, Y.; Chen, P. Y.; Kad, B. K.; Bodde, S. Structural Biological Composites: An Overview. *JOM* **2006**, *58*, 35–41.
- (21) Yaraghi, N. A.; Kisailus, D. Biomimetic Structural Materials: Inspiration from Design and Assembly. *Annu. Rev. Phys. Chem.* **2018**, *69*, 23–57.
- (22) Grunenfelder, L. K.; Herrera, S.; Kisailus, D. Crustacean-Derived Biomimetic Components and Nanostructured Composites. *Small* **2014**, *10*, 3207–3232.
- (23) Ferraro, C.; Garcia-Tuñon, E.; Rocha, V. G.; Barg, S.; Fariñas, M. D.; Alvarez-Arenas, T. E. G.; Sernicola, G.; Giuliani, F.; Saiz, E. Light and Strong SiC Networks. *Adv. Funct. Mater.* **2016**, *26*, 1636–1645.
- (24) Shang, J. S.; Ngerm, N. H. H.; Tan, V. B. C. Crustacean-Inspired Helicoidal Laminates. *Compos. Sci. Technol.* **2016**, *128*, 222–232.
- (25) Compton, B. G.; Lewis, J. A. 3D-Printing of Lightweight Cellular Composites. *Adv. Mater.* **2014**, *26*, 5930–5935.
- (26) Kokkinis, D.; Schaffner, M.; Studart, A. R. Multimaterial Magnetically Assisted 3D Printing of Composite Materials. *Nat. Commun.* **2015**, *6*, 8643.
- (27) Yang, Y.; Chen, Z. Y.; Song, X.; Zhang, Z. F.; Zhang, J.; Shung, K. K.; Zhou, Q. F.; Chen, Y. Biomimetic Anisotropic Reinforcement Architectures by Electrically Assisted Nanocomposite 3D Printing. *Adv. Mater.* **2017**, *29*, 1605750.
- (28) Le Ferrand, H.; Bouville, F.; Niebel, T. P.; Studart, A. R. Magnetically Assisted Slip Casting of Bioinspired Heterogeneous Composites. *Nat. Mater.* **2015**, *14*, 1172–1179.
- (29) Martin, J. J.; Fiore, B. E.; Erb, R. M. Designing Bioinspired Composite Reinforcement Architectures via 3D Magnetic Printing. *Nat. Commun.* **2015**, *6*, 8641.
- (30) Grossman, M.; Bouville, F.; Erni, F.; Masania, K.; Libanori, R.; Studart, A. R. Mineral Nano-Interconnectivity Stiffens and Toughens Nacre-Like Composite Materials. *Adv. Mater.* **2017**, *29*, 1605039.
- (31) Bouville, F.; Maire, E.; Deville, S. Self-Assembly of Faceted Particles Triggered by a Moving Ice Front. *Langmuir* **2014**, *30*, 8656–8663.
- (32) Bai, H.; Chen, Y.; Delattre, B.; Tomsia, A. P.; Ritchie, R. O. Bioinspired Large-Scale Aligned Porous Materials Assembled with Dual Temperature Gradients. *Sci. Adv.* **2015**, *1*, e1500849.
- (33) Deville, S.; Saiz, E.; Tomsia, A. P. Ice-Templated Porous Alumina Structures. *Acta Mater.* **2007**, *55*, 1965–1974.
- (34) Waschkie, T.; Oberacker, R.; Hoffmann, M. J. Control of Lamellae Spacing During Freeze Casting of Ceramics Using Double-Side Cooling as a Novel Processing Route. *J. Am. Ceram. Soc.* **2009**, *92*, S79–S84.
- (35) Gutiérrez, M. C.; Ferrer, M. L.; Del Monte, F. Ice-Templated Materials: Sophisticated Structures Exhibiting Enhanced Functionalities Obtained after Unidirectional Freezing and Ice-Segregation-Induced Self-Assembly. *Chem. Mater.* **2008**, *20*, 634–648.
- (36) Oner Ekiz, O. O.; Dericioglu, A. F.; Kakisawa, H. An Efficient Hybrid Conventional Method to Fabricate Nacre-Like Bulk Nano-Laminar Composites. *Mater. Sci. Eng., C* **2009**, *29*, 2050–2054.
- (37) Song, F.; Bai, Y. L. Effects of Nanostructures on the Fracture Strength of the Interfaces in Nacre. *J. Mater. Res.* **2003**, *18*, 1741–1744.
- (38) Xia, S.; Wang, Z. N.; Chen, H.; Fu, W. X.; Wang, J. F.; Li, Z. B.; Jiang, L. Nanoasperity: Structure Origin of Nacre-Inspired Nanocomposites. *ACS Nano* **2015**, *9*, 2167–2172.
- (39) Khayer Dastjerdi, A. K.; Rabiei, R.; Barthelat, F. The Weak Interfaces within Tough Natural Composites: Experiments on Three Types of Nacre. *J. Mech. Behav. Biomed. Mater.* **2013**, *19*, 50–60.
- (40) Katti, D. R.; Pradhan, S. M.; Katti, K. S. Modeling the Organic-Inorganic Interfacial Nanoasperities in a Model Bio-Nanocomposite, Nacre. *Rev. Adv. Mater. Sci.* **2004**, *6*, 162–168.
- (41) Launey, M. E.; Munch, E.; Alsem, D. H.; Barth, H. B.; Saiz, E.; Tomsia, A. P.; Ritchie, R. O. Designing Highly Toughened Hybrid Composites through Nature-Inspired Hierarchical Complexity. *Acta Mater.* **2009**, *57*, 2919–2932.
- (42) Naglieri, V.; Gludovatz, B.; Tomsia, A. P.; Ritchie, R. O. Developing Strength and Toughness in Bio-Inspired Silicon Carbide Hybrid Materials Containing a Compliant Phase. *Acta Mater.* **2015**, *98*, 141–151.
- (43) Boßelmann, F.; Romano, P.; Fabritius, H.; Raabe, D.; Epple, M. The Composition of the Exoskeleton of Two Crustacea: The

American Lobster *Homarus Americanus* and the Edible Crab *Cancer Pagurus*. *Thermochim. Acta* **2007**, *463*, 65–68.

(44) Jones, R. M. *Mechanics of Composite Materials*, 2nd ed; Taylor & Francis Publications: Philadelphia, 1999.

(45) ASTM E1820-13, *Standard Test Methods for Measurement of Fracture Toughness*; ASTM International, West Conshohocken, PA, 2013.

(46) Bouville, F.; Maire, E.; Meille, S.; De Moortèle, B. V.; Stevenson, A. J.; Deville, S. Strong, Tough and Stiff Bioinspired Ceramics from Brittle Constituents. *Nat. Mater.* **2014**, *13*, 508–514.

(47) Barthelat, F.; Yin, Z.; Buehler, M. J. Structure and Mechanics of Interfaces in Biological Materials. *Nat. Rev. Mater.* **2016**, *1*, 16007.

(48) Ritchie, R. O. Mechanisms of Fatigue Crack Propagation in Metals, Ceramics and Composites: Role of Crack Tip Shielding. *Mater. Sci. Eng., A* **1988**, *103*, 15–28.

(49) Gómez de Salazar, J. M.; Barrena, M. I.; Morales, G.; Matesanz, L.; Merino, N. Compression Strength and Wear Resistance of Ceramic Foams-Polymer Composites. *Mater. Lett.* **2006**, *60*, 1687–1692.

(50) Davies, I. J.; Hamada, H. Flexural Properties of a Hybrid Polymer Matrix Composite Containing Carbon and Silicon Carbide Fibres. *Adv. Compos. Mater.* **2001**, *10*, 77–76.

(51) Avella, M.; Martuscelli, E.; Raimo, M.; Partch, R.; Gangolli, S. G.; Pascucci, B. Polypropylene Reinforced with Silicon Carbide Whiskers. *J. Mater. Sci.* **1997**, *32*, 2411–2416.

(52) Yao, Y. M.; Zhu, X. D.; Zeng, X. L.; Sun, R.; Xu, J. B.; Wong, C. P. Vertically Aligned and Interconnected SiC Nanowire Networks Leading to Significantly Enhanced Thermal Conductivity of Polymer Composites. *ACS Appl. Mater. Interfaces* **2018**, *10*, 9669–9678.

(53) Launey, M. E.; Ritchie, R. O. On the Fracture Toughness of Advanced Materials. *Adv. Mater.* **2009**, *21*, 2103–2110.

(54) Naglieri, V.; Bale, H. A.; Gludovatz, B.; Tomsia, A. P.; Ritchie, R. O. On the Development of Ice-Templated Silicon Carbide Scaffolds for Nature-Inspired Structural Materials. *Acta Mater.* **2013**, *61*, 6948–6957.

(55) Gulbransen, E. A.; Jansson, S. A. The High-Temperature Oxidation, Reduction, and Volatilization Reactions of Silicon and Silicon Carbide. *Oxid. Met.* **1972**, *4*, 181–201.

(56) Schneider, C. A.; Rasband, W. S.; Eliceiri, K. W. NIH Image to ImageJ: 25 Years of Image Analysis. *Nat. Methods* **2012**, *9*, 671–675.

(57) Zhang, L.; Wang, S. G. Correlation of Materials Property and Performance with Internal Structures Evolvement Revealed by Laboratory X-Ray Tomography. *Materials* **2018**, *11*, 1795.

(58) ASTM C1161-13, *Standard Test Method for Flexural Strength of Advanced Ceramics at Ambient Temperature*; ASTM International: West Conshohocken, PA, 2013.

(59) ASTM D5045-99, *Standard Test Methods for Plane-Strain Fracture Toughness and Strain Energy Release Rate of Plastic Materials*; ASTM International: West Conshohocken, PA, 1999.